Coherent control of H^- photodetachment in parallel static electric and magnetic fields

Qiaoling Wang and Anthony F. Starace
Department of Physics and Astronomy, The University of Nebraska, Lincoln, Nebraska 68588-0111
(Received 11 October 1994)

Theoretical calculations of quantum interference effects occurring in photodetachment of H^- with short-pulse lasers in the presence of a uniform static electric field [Q. Wang and A. F. Starace, Phys. Rev. A **48**, R1741 (1993)] are examined in more detail and extended to the case of parallel static electric and magnetic fields. We show that modulation factors characterizing near-threshold cross sections resulting from detachment by relatively long laser pulses may be employed to set the parameters that are most effective for control of detachment cross-section magnitudes with short coherent laser pulses. Use of a static magnetic field to control detached electron wave-packet motion perpendicular to the static field axis is shown to increase greatly the magnitude of quantum interference effects on the cross sections (from 10% of the field-free cross section in an optimized static electric-field case to 50% in a parallel static electric and magnetic-field case). Theoretical dependence of calculated cross sections on laser pulse lengths, time delays, relative phases, frequencies, and classical electron orbit times are presented and discussed in detail.

PACS number(s): 32.80.Fb, 42.50.Vk

I. INTRODUCTION

The field of quantum control of atomic and chemical processes has grown enormously in recent years. In chemical physics beginning in the mid-1980s a number of groups commenced the investigation of controlling molecular dynamics using lasers. In particular, Tannor *et al.* [1–3] investigated the use of short laser pulses to control wave-packet motion along molecular potential curves. Their goal was to control in which final channels the wave packet departs. Brumer and co-workers [4–6] at the same time investigated using quantum interference between simultaneous excitations in molecules. They proposed the performance of two-color experiments, with one frequency being a multiple of the other so that, e.g., one- and three-photon excitation processes populate some of the same final states. They also proposed varying the relative phase of the two transitions in order to control the yield of the final-state products. Experimental realization of the latter scheme has begun [7].

In atomic physics, the field of quantum control of electronic wave packets in Rydberg atoms has burgeoned. The 1991 review article by Alber and Zoller [8] on this topic lists 155 references. A common element of work in this field is to use short laser pulses to create an electronic wave packet in the high Rydberg state energy region. The wave packet is a coherent superposition of a number of atomic (Rydberg level) eigenstates. Alber and Zoller [8] note that such wave packets "provide a bridge between quantum mechanics and the classical concept of the trajectory of a particle" and that "the evolution of these wave packets provides real-time observations of atomic or molecular dynamics." Elucidating such linkages between classical, semiclassical, and quantum dynamics has long been a goal of theoretical atomic and chemical physics [9].

The wave packets that are produced in most numerical and experimental investigations are usually radial wave packets, i.e., a superposition of Rydberg energy levels localized in the radial direction [10]. However, ways to produce angular wave packets using external fields have also been presented [11]. Typically, experiments are of the pump-probe type in which a localized wave packet is excited, moves along its almost-classical trajectory far from the nucleus, and, when it returns to the origin, is either ionized by another laser pulse or else is deexcited back to the ground state. The probe stage of such experiments is required because the Rydberg wave packets are, after all, bound.

Phase coherent effects have also been extensively studied in atoms. Many authors have explored simultaneous single and multiphoton excitation of final states having the same energy [12–15]. They have primarily considered effects of the relative phase of the two excitation processes. Alber, Ritsch, and Zoller [16] have sketched theoretically an experiment in which there are two laser pulses that are delayed with respect to one another and which differ only in their relative phase. The first laser pulse excites a Rydberg wave packet and the second is delayed so that it turns on just as the wave packet produced by the first laser pulse returns to the origin. The relative phases of the two laser pulses determine whether there is constructive or destructive interference between the wave packets produced by each pulse. Noordam, Duncan, and Gallagher [17] have examined theoretically the effect of the phase difference in just such an experiment as that proposed by Alber *et al.* [16]. They predict that Ramsey fringes can be observed.

Relatively few groups have been concerned with Rydberg wave packets in the presence of external fields. Alber has studied theoretically the production of Rydberg wave packets in atoms in the presence of both electric and

magnetic fields in the vicinity of the ionization threshold [18–20]. This work was concerned with the connection of classical and quantum dynamics and the use of the static fields to control wave packet motion. The evolution of Rydberg wave packets in the presence of a static electric field has been explored experimentally by Noordam, van Linden van den Heuvel, and co-workers [21,22]. Finally, Rydberg wave packets in crossed electric and magnetic fields have been studied both theoretically [23] and experimentally [24].

In this paper we present results of theoretical investigations of negative-ion detachment in the presence of parallel static electric and magnetic fields using short-pulse lasers. Unlike Rydberg states, which are bound and require a probe pulse — or else field ionization — to determine the population of the Rydberg state, the study of negative-ion detachment permits a direct observation of the interplay between quantum interference and classical motion. The motion of the electronic wave packet that is produced by the short-pulse laser is controlled by the external static fields. When the packet returns to the origin, the relative phase of a coherent second laser pulse determines the extent of destructive or constructive quantum interference and controls the magnitude of the detachment cross section. Our two-coherent-laser-pulse treatment is similar to those proposed by Refs. [16] and [17] for Rydberg atoms, but we assume a constant (arbitrary) phase difference between the laser pulses for simplicity.

The present paper extends and discusses in more detail our initial results on short-pulse laser detachment of H^- in a static electric field [25]. (A similar theoretical treatment for short-pulse laser detachment of negative ions in a static magnetic field has just recently been presented [26].) Negative-ion detachment in a static electric field leads to quantum interference effects (e.g., cross-section oscillations) near threshold due to the two possible paths for electron detachment along the static field direction: a direct path and a reflected path [27–29]. This interference has been observed [30]. Our wave-packet calculations [25] showed that the quantum interference interpretation of the observed cross-section oscillations in photodetachment of a negative ion in the presence of a static electric field is indeed a fruitful one. Using a single short laser pulse, we reproduced the cross-section oscillations as long as the laser pulse length was longer than the electron reflection time for motion between the negative ion (i.e., the origin) and the static electric-field potential barrier. The observed oscillations arise as a result of interference between old and new laser-excited electronic amplitudes. If, however, the pulse length of the laser is shorter than the electron reflection time, then the laser-excited electronic wave packet gets reflected by the static electric field and returns to the origin *after* the laser pulse is gone. In this case, the cross-section oscillations disappear because there is no new amplitude with which the returning electronic amplitude can interfere.

We extended our single-laser-pulse calculations to include a double laser pulse of the form [25]

$$\vec{E}_L(t) = \{E_0 \exp(-\alpha^2 t^2) \sin\omega t + E_0 \exp[-\alpha^2 (t-\tau)^2] \sin(\omega t + \beta)\}\hat{k}. \quad (1)$$

One sees that such a pulse involves a time delay and phase difference between two coherent laser pulses. (One might be able to realize such a pulse by beam splitting a single laser pulse with subsequent time delay and phase modulation of one of the beams. However, the precise form of the double pulse is not relevant to the essential physics.) The key point of Ref. [25] is that by making the time delay τ between the two pulses equal to the reflection time of the electronic wave packet produced by the first laser pulse, then the second laser pulse can control the amount of the reflected electronic wave packet which escapes down field toward a detector. This control can be achieved by varying the relative phase of the second laser pulse. Thus one can design experiments in which quantum interference phenomena are observed at *fixed* laser frequency as a function of the relative phase of the two laser pulses. This contrasts with conventional experiments which observe such interference only as a function of laser frequency.

While Ref. [25] demonstrated the feasibility of coherent control of a continuum atomic process, the extent of such control in the case of a static electric field is limited by the tendency of laser-excited wave packets in three spatial dimensions to spread out. Hence, even though half the wave-packet amplitude travels in the direction of the increasing static electric-field potential and gets reflected, little of it returns to the origin where it can be modified by another laser pulse. Thus, for the laser frequency of 1 eV used in the calculations in Ref. [25], the magnitude of the quantum interference effects is of the order of a few percent of the detachment cross section. Calculations presented in this paper with smaller laser frequencies give larger effects of the order of 10%. However, to achieve a major increase in the magnitude of the interference effects requires that one control the extent of wave-packet spreading in three dimensions.

The case of parallel static electric and magnetic fields is an ideal one for this purpose. In this field configuration the electronic wave-packet amplitude is confined by the magnetic field in the direction perpendicular to the static electric field. Furthermore, a new feature is that there are now two time parameters for the system: the reflection time for motion along the electric-field direction and the reflection time for motion perpendicular to this direction. For the infinitely long laser pulse case, the work of Reinhardt [28] as well as the perturbative treatments of Du [31] and of Fabrikant [32] found extremely strong quantum interference effects as large as nearly 100% of the average detachment cross section as a function of laser frequency. Similar results have recently been reported by Peters and Delos [33]. We show here that such effects can be controlled with short laser pulses and observed at fixed frequency as a function of the relative phase of the two laser pulses.

In Sec. II we present our theoretical formulation, which is based on an analytic three-dimensional wave function for a detached electron moving in a laser field and parallel static electric and magnetic fields. Formulas are derived for the H^- detachment transition rate and, in the limit of weak laser intensities, for the detachment cross section and modulation factors. The limiting cases of pure static

electric and magnetic fields are also presented. In Sec. III we first present more detailed results for the static electric-field case considered in Ref. [25]. We then present our results for the parallel static electric- and magnetic-field case. In Sec. IV we discuss our results and adduce some conclusions.

II. THEORETICAL FORMULATION

Our calculations employ an analytic solution of the time-dependent, three-dimensional Schrödinger equation for a detached electron moving in parallel static electric and magnetic fields as well as in the field of a laser pulse. We thereby generalize prior treatments for an electron moving in a monochromatic laser field and either a static magnetic [34] or electric field [35]. These wave functions are in essence the natural extensions of the Volkov solution [36] for an electron in a laser field. As discussed below, our choice of initial-state representation enables us to define a gauge-invariant S matrix. For this reason, we choose the gauges which are most convenient for the external static and laser fields. Finally, in order to compare with prior results employing perturbative treatments for monochromatic laser pulses, we examine the weak laser field, long-pulse limit of our analytic formulas. Throughout this paper we employ atomic units (i.e., $e = \hbar = m = 1$) unless otherwise specified.

A. Analytic final-state wave functions

Consider an electron moving in a static electric field $\vec{E}_S = E_S\hat{k}$, a static magnetic field $\vec{B} = B\hat{k}$, and the field of a laser pulse

$$\vec{E}_L(t) = E_0 e^{-\alpha^2 t^2}(\sin\omega t)\hat{k}, \tag{2}$$

where ω is the laser frequency and the Gaussian factor describes the pulse shape. Introducing the vector potentials

$$\vec{A}_B \equiv Bx\hat{j}, \tag{3}$$

$$\vec{A}_L(t) \equiv -c\int^t \vec{E}_L(t')dt', \tag{4}$$

the time-dependent Schrödinger equation for the final-state wave function in momentum space is

$$\frac{i\hbar\partial\psi(\vec{p},t)}{\partial t} = \left\{\frac{1}{2}\left(\vec{p}+\frac{1}{c}\left[\vec{A}_L+\vec{A}_B\right]\right)^2 + iE_S\frac{\partial}{\partial p_z}\right\}\psi(\vec{p},t) \tag{5a}$$

$$= (H_\perp + H_\parallel)\psi(\vec{p},t), \tag{5b}$$

where

$$H_\perp \equiv \frac{1}{2}\left(p_x^2+p_y^2\right) + i\omega_c p_y\frac{\partial}{\partial p_x} - \frac{1}{2}\omega_c^2\frac{\partial^2}{\partial p_x^2} \tag{6}$$

and

$$H_\parallel \equiv \frac{1}{2}p_z^2 + \frac{1}{c}A_L p_z + \frac{1}{2c}A_L^2 + iE_S\frac{\partial}{\partial p_z}. \tag{7}$$

Note that in Eq. (6) we have introduced the cyclotron frequency

$$\omega_c \equiv B/c. \tag{8}$$

The solution of Eq. (5) is separable. Thus we write

$$\psi(\vec{p},t) \equiv \psi_\perp(p_x,p_y,t)\psi_\parallel(p_z,t), \tag{9}$$

where $\psi_\perp$ ($\psi_\parallel$) is the solution of the time-dependent Schrödinger equation corresponding to $H_\perp$ ($H_\parallel$). For $\psi_\parallel$ we find

$$\psi_\parallel(p_z,t) = (2\pi E_S)^{-1/2}\exp\Big\{-i\epsilon_z t + iE_S^{-1}[p_z^3/6 - \epsilon_z p_z] - i\frac{p_z}{c}\int^t A_L(t')dt' - if(t)\Big\}. \tag{10}$$

In this equation, ϵ_z is the electron's total energy of motion along the z axis, the next two terms in the exponential describe the electron's motion in the static electric field, the fourth term is one of the (Volkov) phases due to the laser field, and the last term is defined as

$$f(t) \equiv (2c^2)^{-1}\int^t A_L^2(t')dt' + \frac{E_S}{c}\int^t dt'\left[\int^{t'} dt'' A_L(t'')\right]. \tag{11}$$

The first term in Eq. (11) leads to another (Volkov) phase due to the laser field plus a ponderomotive shift and the second term represents a coupling of the static electric and laser fields [35]. The factor outside the exponential in Eq. (10) gives $\psi_\parallel$ a normalization per unit energy. The solution defined by Eqs. (10) and (11) has been considered in detail in Refs. [25] and [35].

For $\psi_\perp(p_x,p_y,t)$ we find

$$\psi_\perp(p_x,p_y,t) = \delta(p_y-k_y)\exp[i(k_y p_x/\omega_c - \epsilon_\perp t)]\Phi_n(p_x), \tag{12}$$

where the energy $\epsilon_\perp$ is

$$\epsilon_\perp \equiv (n+1/2)\omega_c, \tag{13}$$

and $\Phi_n(p_x)$ is the momentum-space solution for a one-dimensional harmonic oscillator [37]

$$\Phi_n(p_x) \equiv [2^n n!(\pi\omega_c)^{1/2}]^{-1/2}e^{-p_x^2/(2\omega_c)}H_n(p_x\omega_c^{-1/2}), \tag{14}$$

where H_n is the nth degree Hermite polynomial. $\psi_\perp$ is normalized per unit momentum in p_y and to unity in p_x.

In summary, the momentum-space wave function for an electron moving in a laser field [defined by Eqs. (2) and (4)] and parallel static electric (E_S) and magnetic (B) fields is given by Eqs. (9), (10), and (12) as

$$\psi_{nk_y\epsilon_z}(p_x,p_y,p_z,t)$$

$$= \Phi_n(p_x)\delta(p_y-k_y)(2\pi E_S)^{-1/2} \times \exp\Big[i\Big(-\epsilon_f t + k_y p_x \omega_c^{-1} + E_S^{-1}[p_z^3/6 - \epsilon_z p_z] - (p_z/c)\int^t A_L(t')\,dt' - f(t)\Big)\Big], \quad (15)$$

where $f(t)$ and $\Phi_n(p_x)$ are defined by Eqs. (11) and (14), respectively, and where the energy ϵ_f is defined by

$$\epsilon_f \equiv \epsilon_\perp + \epsilon_z = (n+1/2)\omega_c + \epsilon_z. \quad (16)$$

The coordinate space wave function in x and z is obtained by taking the Fourier transform of Eq. (15) to get

$$\psi_{nk_y\epsilon_z}(x,p_y,z,t)$$

$$= e^{-i\epsilon_f t - if(t)}\phi_n(x+k_y\omega_c^{-1})\delta(p_y-k_y) \times (4/E_S)^{1/6}\mathrm{Ai}\Big((2E_S)^{1/3}\Big(z-\epsilon_z/E_S - c^{-1}\int^t A_L(t')dt'\Big)\Big). \quad (17)$$

In this equation $f(t)$ and ϵ_f are defined in Eqs. (11) and (16), respectively, Ai is the regular Airy function, and ϕ_n is defined by

$$\phi_n\Big(x+k_y\omega_c^{-1}\Big)$$

$$\equiv i^n\Big[\omega_c^{1/2}/(\pi^{1/2}2^n n!)\Big]^{1/2} \times \exp[-(x+k_y\omega_c^{-1})^2\omega_c/2]H_n\Big(\omega_c^{1/2}(x+k_y\omega_c^{-1})\Big). \quad (18)$$

B. Initial-state wave function

We choose our initial-state wave function to be the Ohmura-Ohmura [38] wave function for H^-. It is given in momentum space by

$$\psi_i(\vec{p},t) = \frac{b}{(2\pi)^{1/2}}\frac{1}{(p^2/2-\epsilon_i)}e^{-i\epsilon_i t}. \quad (19)$$

The form of this wave function is a well-known approximation for a weakly bound electron which stems from the effective range theory for an s electron [39]. Using the variational results of Ref. [38] for H^- and the effective range theory [39], one finds [40]

$$b = 0.315\,52 \quad (20a)$$

and

$$\epsilon_i = -0.027\,751 \text{ a.u.} \quad (20b)$$

C. S matrix

The form of the S matrix for detachment of H^- in the presence of parallel static electric and magnetic fields depends on our choices for the initial- and final-state wave functions. Specifically, our initial-state wave function in Eq. (19) is assumed to be a solution of the atomic Hamiltonian for H^-; that is, we assume that the static fields are sufficiently weak that they do not distort the initial-state wave function. The final-state wave function in Eq. (15) describes exactly the detached electron's motion in all external fields except that of the residual atom. Ignoring the electron-atom final-state interaction is a common approximation in H^- detachment in external static fields [35].

For these choices of initial- and final-state wave functions, the S matrix element for a transition between them is

$$S_{nk_y\epsilon_z} = -i\int_{-\infty}^{+\infty}\langle\psi_{nk_y\epsilon_z} \mid H_I \mid \psi_i\rangle dt, \quad (21)$$

where H_I comprises all of the field-dependent terms (i.e., those involving ω_c, E_S, and A_L) in Eqs. (6) and (7). As shown in Sec. III A of Ref. [35], for initial states of the form of Eq. (19), this S-matrix element is gauge invariant and equal to [cf. Eq. (27) of Ref. [35]]

$$S_{nk_y\epsilon_z} = +i\int_{-\infty}^{\infty}\langle\psi_{nk_y\epsilon_z} \mid b(2\pi)^{-1/2}\rangle e^{-i\epsilon_i t}dt. \quad (22)$$

Carrying out the momentum-space integrations in Eq. (22), we obtain

$$S_{nk_y\epsilon_z}(t) = i(2\pi)^{1/2}b\ \phi_n(-k_y\omega_c^{-1})I_{n\epsilon_z}(t), \quad (23a)$$

where

$$I_{n\epsilon_z}(t) \equiv (4/E_S)^{1/6}\int_{-\infty}^{t}dt'\exp i\Big[(\epsilon_f-\epsilon_i)t' + f(t')\Big] \times \mathrm{Ai}\Big(-(2E_S)^{1/3}\Big(\frac{\epsilon_z}{E_S}+\frac{1}{c}\int^{t'}dt''A_L(t'')\Big)\Big). \quad (23b)$$

The S matrix in Eq. (22) is the limit of Eq. (23) as $t \to +\infty$; it is convenient to define a time-dependent S-matrix element in order to examine wave-packet behavior while the laser pulse is on.

D. Wave-packet amplitude

We may use the time-dependent transition amplitude in Eq. (23) to determine the temporal and spatial behavior (in x and z) of the detached electron's probability

amplitude as follows:

$$\psi_{\rm WP}(x,p_y,z,t) = \sum_{n=0}^{\infty}\int_{-\infty}^{+\infty} dk_y \int_{-\infty}^{+\infty} d\epsilon_z \psi_{nk_y\epsilon_z}(x,p_y,z,t) S_{nk_y\epsilon_z}(t). \tag{24}$$

In words, Eq. (24) defines the wave-packet amplitude as a sum over all final states of the product of the transition amplitude to each final state (n,k_y,ϵ_z) at a particular time t and the wave function in Eq. (17) for that final state. Substituting Eqs. (17) and (23) into Eq. (24) and making use of Eq. (16), we obtain

$$\psi_{\rm WP}(x,p_y,z,t) = ib(2\pi)^{1/2} e^{-if(t)} \sum_{n=0}^{\infty} \phi_n(x+k_y\omega_c^{-1})\phi_n(-k_y\omega_c^{-1}) e^{-i(n+1/2)\omega_c t}(4/E_S)^{1/6} \times \int_{-\infty}^{+\infty} d\epsilon_z e^{-i\epsilon_z t} {\rm Ai}\left((2E_S)^{1/3}\left(z-\epsilon_z/E_S - c^{-1}\int^t A_L(t')dt'\right)\right) I_{n\epsilon_z}(t). \tag{25}$$

E. Cross sections

The transition rate to a particular final state (n,k_y,ϵ_z) is

$$W_{nk_y\epsilon_z} = (2\pi)^{-1}|S_{nk_y\epsilon_z}|^2 = b^2|\phi_n(-k_y\omega_c^{-1})|^2\,|I_{n\epsilon_z}|^2. \tag{26}$$

In Eq. (26),

$$I_{n\epsilon_z} \equiv \lim_{t\to\infty} I_{n\epsilon_z}(t), \tag{27}$$

where $I_{n\epsilon_z}(t)$ is defined in Eq. (23b). The total cross section may be calculated from the transition rate $W_{nk_y\epsilon_z}$:

$$\sigma = F^{-1}\sum_{n=0}^{\infty}\int_{-\infty}^{+\infty} dk_y \int_{-\infty}^{+\infty} d\epsilon_z\, W_{nk_y\epsilon_z} = F^{-1}b^2\omega_c \sum_{n=0}^{\infty}\int_{-\infty}^{\infty} d\epsilon_z |I_{n\epsilon_z}|^2. \tag{28}$$

To obtain the second line in Eq. (28), use is made of the normalization integral for Hermite polynomials [41]. F is the incident flux. Appropriate values for F for short laser pulses are obtained in the next subsection. It is useful to define the partial cross section for the nth Landau threshold:

$$\sigma = \sum_n \sigma_n, \tag{29a}$$

where

$$\sigma_n \equiv F^{-1}b^2\omega_c \int_{-\infty}^{\infty} d\epsilon_z |I_{n\epsilon_z}|^2. \tag{29b}$$

F. Fluxes for single and double Gaussian laser pulses

Consider first the Gaussian-shaped laser pulse defined in Eq. (2). We may Fourier analyze it, i.e., set

$$E_L(t) \equiv \int_{-\infty}^{+\infty} \tilde{E}(\Omega) e^{i\Omega t} d\Omega. \tag{30}$$

One finds for the frequency-dependent amplitude $\tilde{E}(\Omega)$ [after substituting Eq. (2) in Eq. (30) and Fourier transforming both sides]

$$\tilde{E}(\Omega) = \frac{E_0}{4\pi^{1/2}i\alpha}\left(\exp\left[-\frac{(\Omega-\omega)^2}{4\alpha^2}\right] - \exp\left[-\frac{(\Omega+\omega)^2}{4\alpha^2}\right]\right). \tag{31}$$

We define the total intensity $I_{\rm tot}$ of the laser pulse as the integrated intensity of each frequency component

$$I_{\rm tot} = \frac{c}{4\pi}\int_{-\infty}^{+\infty} |\tilde{E}(\Omega)|^2 d\Omega. \tag{32}$$

Dropping the cross terms in $|\tilde{E}(\Omega)|^2$ since they are always negligible compared to the other two terms (for $\omega/\alpha \gg 1$), we find, after performing the integral over Ω,

$$I_{\rm tot} = \frac{cE_0^2}{8\pi}\left[2\alpha(2\pi)^{1/2}\right]^{-1}. \tag{33}$$

The flux for a single Gaussian pulse defined by Eq. (2) is thus

$$F_1 \equiv I_{\rm tot}/\omega = \frac{cE_0^2}{8\pi\omega}[2\alpha(2\pi)^{1/2}]^{-1}. \tag{34}$$

One notices immediately that the plane-wave limit (i.e., $\alpha \to 0$) gives a singular flux. However, if one substitutes Eq. (34) in the cross-section formula in Eq. (28) first, then the limit as $\alpha \to 0$ is finite and, as expected, is equal to the plane-wave laser result, as we show in the next subsection.

The flux for a double Gaussian pulse [such as that defined in Eq. (1) in which the second pulse is delayed by a time τ and shifted by the relative phase β] may be similarly calculated. Substituting Eq. (1) in Eq. (30), we obtain

$$\tilde{E}(\Omega) = \frac{E_0}{4\pi^{1/2}i\alpha}\left\{\exp\left[-\frac{(\Omega-\omega)^2}{4\alpha^2}\right](1+e^{i(\omega-\Omega)\tau+i\beta}) - \exp\left[-\frac{(\Omega+\omega)^2}{4\alpha^2}\right](1+e^{-i(\omega+\Omega)\tau-i\beta})\right\}. \tag{35}$$

Substituting Eq. (35) into Eq. (32), dropping the cross terms because of the small factor $\exp[-(\omega^2+\Omega^2)/4\alpha^2]$, and integrating over frequency, we obtain, for the flux for the double Gaussian pulse defined in Eq. (1),

$$F_2 \equiv \frac{I_{\rm tot}}{\omega} = \frac{cE_0^2}{8\pi\omega}[(2\pi)^{1/2}\alpha]^{-1}[1+\cos\beta\exp(-\alpha^2\tau^2/2)]. \tag{36}$$

G. The weak laser, long-pulse limit for the cross section

In order to compare our results with results of perturbative calculations employing monochromatic laser excitation, we must examine the weak laser, long-pulse limit of our formulas for the cross section [cf. Eqs. (28) and (29)]. It turns out that typically employed experimental values for laser pulse duration and intensity fall in the weak laser, long-pulse limit and thus predictions employing such limiting values have relevance to current experimental capabilities.

We focus on the amplitudes $I_{n\epsilon_z}$ defined by Eqs. (23b) and (27) since this amplitude determines the total and partial cross sections according to Eqs. (28) and (29). In the weak laser limit, i.e., $E_0 \to 0$ [cf. Eq. (2)], we retain only terms in Eq. (23b) that are of first order in E_0. Thus we expand the exponential in Eq. (23b) to first order in $f(t')$ [and keep only the second integral in Eq. (11)] and expand the Airy function in Eq. (23b) to first order in A_L [cf. Eq. (4)]. Thus

$$\lim_{E_0\to 0} I_{n\epsilon_z} = (4/E_S)^{1/6}\int_{-\infty}^{+\infty} dt\exp[i(\epsilon_f-\epsilon_i)t] \times\left[i\frac{E_S}{c}\mathrm{Ai}(-\xi)\int^t dt'\int^{t'} dt'' A_L(t'') - \frac{(2E_S)^{1/3}}{c}Ai'(-\xi)\int^t dt' A_L(t')\right], \tag{37}$$

where we have introduced the scaled energy variable

$$\xi \equiv (2E_S)^{1/3}\epsilon_z/E_S. \tag{38}$$

For the typical case that $\alpha/\omega \ll 1$ (i.e. , that the pulse shape is not too short), the time integrals of A_L over the t' and t'' in Eq. (37) may be performed using integration by parts (dropping all terms of order α/ω or higher). The integral over t may then be carried out to obtain

$$\lim_{\alpha/\omega\to 0, E_0\to 0} I_{n\epsilon_z} = \frac{-iE_0}{\omega^2}\pi\delta_\alpha(\epsilon_f-\epsilon_i-\omega)(4/E_S)^{1/6} \times\left[\frac{E_S}{\omega}\mathrm{Ai}(-\xi)+(2E_S)^{1/3}\mathrm{Ai}'(-\xi)\right], \tag{39}$$

where we have introduced the quasi-δ-function

$$\delta_\alpha(\epsilon_f-\epsilon_i-\omega) = (2\pi^{1/2}\alpha)^{-1}\exp[-(\epsilon_f-\epsilon_i-\omega)^2/4\alpha^2]. \tag{40}$$

In the limit that our finite laser pulse becomes a monochromatic plane wave, the quasi-δ-function becomes the usual Dirac δ function

$$\delta(\epsilon_f-\epsilon_i-\omega) = \lim_{\alpha\to 0}\delta_\alpha(\epsilon_f-\epsilon_i-\omega). \tag{41}$$

Substituting Eq. (39) into Eq. (28) and using the single laser pulse flux given in Eq. (34), we obtain, for the total cross section,

$$\sigma = \frac{8\pi^3 b^2\omega_c}{c\omega^3}\sum_{n=0}^{\infty}\int_{-\infty}^{+\infty} d\epsilon_z\bar{\delta}_\alpha(\epsilon_f-\epsilon_i-\omega) \times(4/E_S)^{1/3}\left[\frac{E_S}{\omega}\mathrm{Ai}(-\xi)+(2E_S)^{1/3}\mathrm{Ai}'(-\xi)\right]^2, \tag{42}$$

where another quasi-δ-function has been introduced,

$$\bar{\delta}_\alpha(\epsilon_f-\epsilon_i-\omega) \equiv (8\pi)^{1/2}\alpha\delta_\alpha^2 = (2^{1/2}\pi^{1/2}\alpha)^{-1} \times\exp[-(\epsilon_f-\epsilon_i-\omega)^2/2\alpha^2]. \tag{43}$$

As with δ_α, we have

$$\delta(\epsilon_f-\epsilon_i-\omega) = \lim_{\alpha\to 0}\bar{\delta}_\alpha(\epsilon_f-\epsilon_i-\omega). \tag{44}$$

In the limit of a monochromatic laser (i.e., $\alpha \to 0$), the integral over ϵ_z in Eq. (42) fixes ϵ_z and hence ξ, which becomes [cf. Eqs. (38) and (16)]

$$\lim_{\alpha\to 0}\xi \equiv \xi_0 = (2E_S)^{1/3}[\epsilon_i+\omega-\omega_c(n+1/2)]/E_S. \tag{45}$$

Thus

$$\lim_{\alpha\to 0}\sigma = \frac{8\pi^3 b^2\omega_c}{c\omega^3}\sum_{n=0}^{\infty}(4/E_S)^{1/3} \times\left[\frac{E_S}{\omega}\mathrm{Ai}(-\xi_0)+(2E_S)^{1/3}\mathrm{Ai}'(-\xi_0)\right]^2. \tag{46}$$

The weak laser, long-pulse limit for the case of the double laser pulse in Eq. (1) may be analyzed similarly. Thus the amplitudes $I_{n\epsilon_z}^{(d)}$, where the d indicates the double pulse case, equal

$$\lim_{\alpha/\omega\to 0, E_0\to 0} I_{n\epsilon_z}^{(d)} = I_{n\epsilon_z}\{1+\exp[-i\beta+i(\epsilon_f-\epsilon_i-\omega)\tau]\}, \tag{47}$$

where $I_{n\epsilon_z}$ in Eq. (47) is given by Eq. (39). The cross section for the double laser pulse case may be obtained by substituting Eq. (47) into Eq. (28) and using the double laser pulse flux given in Eq. (36).

H. Modulation factor

The influence of the parallel E_S and B fields on the H^- photodetachment cross section near threshhold may be demonstrated most clearly by calculation of a modulation factor H, which multiplies the field-free detachment cross section for H^-, σ_0,

$$\sigma = H(E_S,B)\sigma_0. \tag{48}$$

Near threshold, the field-free cross section is [42]

$$\sigma_0 = \left(\frac{8\pi^3 b^2}{c\omega^3}\right)\left(\frac{8^{1/2}}{3\pi}\right)(\omega+\epsilon_i)^{3/2}, \tag{49}$$

which clearly exhibits the Wigner threshold law [43]. Thus, for example, for the case of parallel static electric and magnetic fields and a single laser pulse [defined by Eq. (2)], the modulation factor $H(E_S,B)$ can be calculated from Eq. (48) using Eq. (42) for the cross section σ. In the long-pulse limit, Eq. (46) may be used for σ to obtain

$$\lim_{\alpha\to 0} H(E_S,B) = \frac{3}{2}\omega_c\left(\frac{\pi}{2^{1/2}}\right)\left(\frac{4}{E_S}\right)^{1/3}(\omega+\epsilon_i)^{-3/2} \times \sum_{n=0}^{\infty}\left[\frac{E_S}{\omega}\mathrm{Ai}(-\xi_0)+(2E_S)^{1/3}\mathrm{Ai}'(-\xi_0)\right]^2, \tag{50}$$

where ξ_0 is defined by Eq. (45).

I. Pure magnetic- or electric-field case

It is of interest to examine the limiting cases of Eq. (42) in which either the electric or the magnetic field is zero. Consider first the case that $E_S \to 0$. In this case the scaled variable ξ [cf. Eq. (38)] becomes infinite and hence the Airy function and its derivative take their asymptotic values [44]. Dropping the Airy function term in comparison with that involving its derivative and taking the average value of the squared cosine function, we obtain, for the case of a single laser pulse [cf. Eq. (2)],

$$\sigma_B = \frac{8\pi^2 b^2}{c\omega^3}2^{1/2}\omega_c\sum_{n=0}^{\infty}\int_0^{\infty} d\epsilon_z\,\epsilon_z^{1/2}\bar{\delta}_\alpha(\epsilon_f-\epsilon_i-\omega), \tag{51}$$

where $\bar{\delta}_\alpha$ is defined by Eq. (43) and ϵ_f is defined by Eq. (16). The long-pulse limit of Eq. (51) agrees with the weak laser field limit of Eq. (A7) of Ref. [34].

Consider now the case that $B \to 0$. In this case the summation over n may be replaced by an integral, i.e.,

$$\lim_{B\to 0}\omega_c\sum_{n=0}^{\infty} = \int_0^{\infty}\omega_c dn = \int_0^{\infty} d\epsilon_\perp, \tag{52}$$

where the last equality follows from Eq. (16). Thus, Eq. (42) becomes

$$\sigma_{E_S} = \frac{8\pi^3 b^2}{c\omega^3}\int_0^{\infty} d\epsilon_\perp \int_{-\infty}^{+\infty} d\epsilon_z \bar{\delta}_\alpha(\epsilon_f-\epsilon_i-\omega) \times\left(\frac{4}{E_S}\right)^{1/3}\left[\frac{E_S}{\omega}\mathrm{Ai}(-\xi)+(2E_S)^{1/3}\mathrm{Ai}'(-\xi)\right]^2, \tag{53}$$

where ϵ_f is defined by Eq. (16) and $\xi(\epsilon_z)$ is defined by Eq. (38). The long-pulse limit of Eq. (53) agrees with Eq. (64) of Ref. [35].

III. RESULTS

We show here how experimentally controlled parameters for incident laser pulse shapes determine the magnitudes of H^- photodetachment cross sections in external static fields. We employ two basic laser pulse shapes: a single and a double Gaussian pulse, which are described by Eqs. (2) and (1), respectively. These are illustrated in Fig. 1 for a particular set of parameters. In what follows, we present further results for the pure static electric-field case that was considered in Ref. [25]. We then present results for the parallel static electric- and magnetic-field case.

A. Pure static electric-field case

As discussed in Ref. [25], the quantum mechanical interference that is exhibited by the oscillations in the cross section for detachment of H^- in the presence of a static electric field is sensitive to the duration of the finite laser pulse. Briefly, the detached electron probability amplitude can escape along the negative z axis by either of two paths: a direct path (in which the electron travels initially "down field" along the negative z axis) and a reflected path (in which the electron travels initially "up field" along the positive z axis and is reflected at the classical turning point, subsequently escaping along the negative z axis). Quantum interference occurs between the "reflected path" electron probability amplitude that returns to the origin at $z = 0$ and the "direct path" electron probability amplitude that is being newly produced at $z = 0$ by the laser pulse. As demonstrated in Ref. [25], cross-section oscillations may be observed as long as the laser pulse duration is longer than the reflection time for an electron wave packet.

1. Modulation factor dependence on laser pulse duration

In Fig. 2 we show the cross-section modulation factor H [cf. Eqs. (48) and (49)] corresponding to the cross sec-

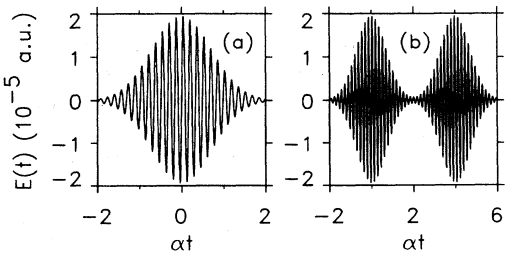

FIG. 1. (a) Gaussian-shaped single laser pulse defined by Eq. (2). (b) Double laser pulse defined by Eq. (1). The pulses shown have a peak amplitude $E_0 = 10^5$ V/cm, frequency $\omega = 0.84$ eV, and pulse width $2/\alpha = 0.06$ psec. The double pulse in (b) has a pulse separation $\tau = 4/\alpha$ and a relative phase $\beta = 0$.

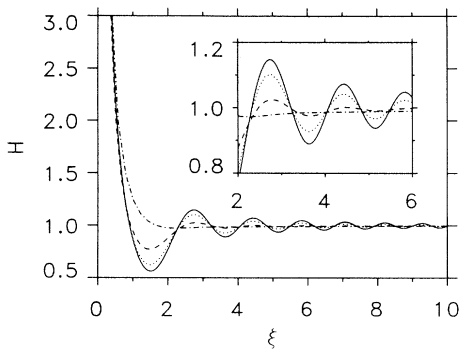

FIG. 2. Modulation factors H [cf. Eqs. (48) and (49)] for photodetachment of H^- by a linearly polarized Gaussian laser pulse [cf. Eq. (2)] in the presence of a static electric field $\vec{E}_S = 1.64$ V/cm $\hat{k}$. H is plotted vs the scaled energy variable $\xi \equiv (2/E_S^2)^{1/3}(\omega + \epsilon_i)$ [cf. Eq. (38)] for four values of the laser pulse width $(2/\alpha)$: 1 psec (solid curve), 0.24 psec (dotted curve), 0.12 psec (dashed curve), and 0.06 psec (dash-dotted curve). The inset shows H on an expanded scale in the range $2 \leq \xi \leq 6$.

tion in Eq. (53) for four values of the laser pulse duration. H is plotted as a function of the scaled energy variable ξ defined in Eq. (38). The magnitude of the static electric field used is $E_S = 1.64 \times 10^5$ V/cm. The curves shown are those for laser pulse widths $2/\alpha = 1.00$ psec, 0.24 psec, 0.12 psec, and 0.06 psec. For $2/\alpha = 1.0$ psec, the oscillations of the modulation factor $H(\xi)$ are essentially those of a monochromatic laser pulse, while for $2/\alpha = 0.06$ psec, the oscillations have vanished.

Figure 2 may be understood using classical arguments. According to Newtonian mechanics, the reflection time for an electron in a static electric field E_S is

$$T_E \equiv (2/E_S)[2(\omega + \epsilon_i - \epsilon_\perp)]^{1/2}. \tag{54}$$

The amplitude that returns to the origin is that for which $\epsilon_\perp = 0$. For the static field E_S at which the calculations in Fig. 2 were performed, the scaled energy variable $\xi = 1$ corresponds to a laser frequency $\omega = 0.777$ eV. The classical reflection time for this frequency is 0.06 psec. This classical reflection time is equal to the shortest laser pulse width employed in Fig. 2. Hence, for this case, the laser pulse is just about over at the time the reflected electron probability amplitude produced by the first half of the laser pulse returns to the origin. At larger values of ξ (and hence ω), the classical reflection time is even longer. Hence, for a laser pulse width $2/\alpha \leq 0.06$ psec, we expect the cross-section oscillations to disappear.

2. *Time development of detached electron wave packets*

This classical interpretation is verified by our quantum-mechanical wave-packet calculations shown in Fig. 3. In this figure we plot the detached electron wave-packet probability density $|\psi_{WP}(p_x, p_y, z, t)|^2$ for the case $p_x = p_y = 0$ as a function of z and t. [$\psi_{WP}(p_x, p_y, z, t)$ is defined by Eq. (6) of Ref. [25] and corresponds to the parallel static electric and magnetic fields wave packet defined in Eq. (24) above.] In order to relate the time development of the detached electron wave packet to the passage of the laser pulse over the H^- ion, we measure time in units of $1/\alpha$. Our single laser pulse, which is described by Eq. (2) and exhibited in Fig. 1(a), has a width of $2/\alpha = 0.06$ psec and a frequency of $\omega = 0.84$ eV. Figure 3 shows that at $t = -1/\alpha$ [cf. Fig. 3(a)] the wave packet has very little amplitude, whereas at $t = 0$ [cf. Fig. 3(b)] the wave packet is bifurcating, with half the amplitude heading toward negative values of z and half heading toward positive values of z. The latter group, however, is trapped by the Stark potential, while the former group escapes [cf. Fig. 3(d)]. Figures 3(e)–3(h) show that long after the laser pulse has swept past the H^- ion at $t = 2/\alpha$, the probability amplitude trapped by the Stark potential returns to the origin at $z = 0$ [cf. Fig. 3(f)] and eventually escapes along the negative z axis [cf. Fig. 3(h)], much as the direct path wave packet does [cf. Fig. 3(d)], but delayed by the reflection time of $\approx 4/\alpha = 0.12$ psec for this laser frequency.

Figure 4 demonstrates how one can partially control the magnitude of the detached electron probability amplitude which escapes along the negative z axis by employing a coherent, double laser pulse of the kind defined

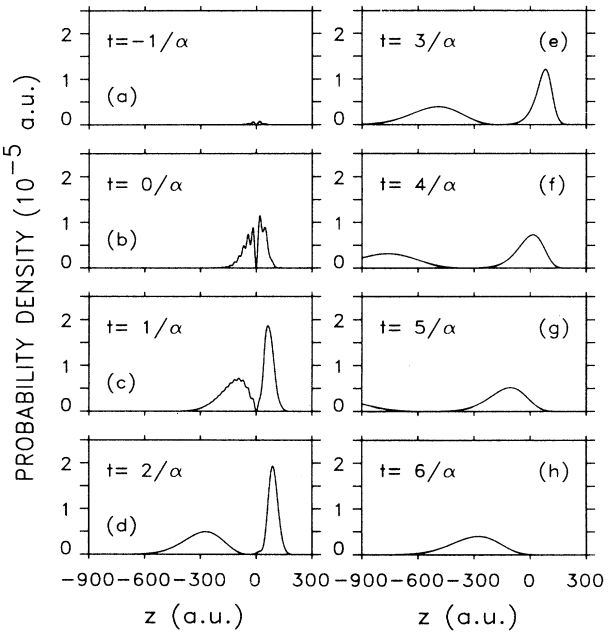

FIG. 3. Wave-packet probability $|\psi_{WP}(p_x, p_y, z, t)|^2$ for $p_x = p_y = 0$ for electrons detached from H^- in a static electric field ($\vec{E}_S = 1.64 \times 10^5$ V/cm $\hat{k}$) by a laser pulse of frequency $\omega = 0.84$ eV linearly polarized along $\hat{k}$ and having the form in Fig. 1(a), where the width is $2/\alpha = 0.06$ psec. (a)–(h) show the electronic wave-packet distribution along the z axis for times t measured in units of $1/\alpha$. The laser pulse passes over the H^- ion for $-2/\alpha \leq t \leq 2/\alpha$; for $t > 2/\alpha$ the electronic wave packet moves only under the influence of the static field.

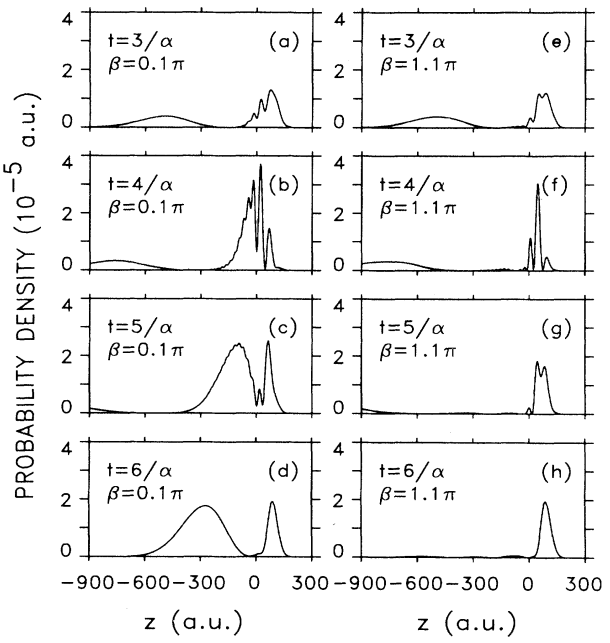

FIG. 4. Same as Fig. 3, but for the double laser pulse shown in Fig. 1(b), with each laser pulse having a width $2/\alpha = 0.06$ psec and frequency $\omega = 0.84$ eV. The time delay between pulses is $\tau = 4/\alpha = 0.12$ psec and their relative phase is β. The first laser pulse passes over the H^- atom during $-2/\alpha \leq t \leq 2/\alpha$ and produces a wave-packet distribution identical to that in Fig. 3. The second laser pulse passes over the H^- ion during $+2/\alpha \leq t \leq +6/\alpha$. (a)–(d) show the case of constructive interference ($\beta = 0.1\pi$) and (e)–(h) show the case of destructive interference ($\beta = 1.1\pi$).

by Eq. (1) and exhibited in Fig. 1(b). The two laser pulses have a separation $\tau = 4/\alpha$ equal to the wave-packet reflection time; their relative phase is $\beta = 0.1\pi$ in Figs. 4(a)–4(d) and $\beta = 1.1\pi$ in Figs. 4(e)–4(h). The relative phase $\beta = 0.1\pi$ leads to constructive interference between the reflected path electron probability amplitude produced by the first laser pulse and the direct path electron probability amplitude produced by the second laser pulse. The relative phase $\beta = 1.1\pi$, on the other hand, leads to destructive interference between these two amplitudes. [Note that the reflected path probability amplitude produced by the second laser pulse will, in each case, proceed eventually toward negative z; e.g., there will be a probability distribution similar to that shown in Fig. 3(h) for $t = 10/\alpha$.]

3. Dependence of the detachment cross section on the relative phase of two short laser pulses

Different choices of p_x and p_y will produce interference effects such as those shown in Fig. 4 only for different values of β. The measured cross section is the result of an integration over $\epsilon_\perp \equiv (p_x^2 + p_y^2)/2$, as shown in Eq. (53). Because of this integration, the effect of such quantum interference on the cross section is of smaller magnitude than for a particular wave-packet trajectory. This is shown in Fig. 5, which presents the cross section for detachment of H^- as a function of the relative phase β of a double laser pulse of the form in Eq. (1) with $\omega = 0.84$ eV and $\tau = 4/\alpha = 0.12$ psec. One sees that in varying β over 2π degrees, the cross section at fixed laser frequency $\omega = 0.84$ eV varies by about 10% from peak to trough.

Two general observations may be made concerning the magnitude of the cross-section oscillations as a function of the relative phase β. First, the magnitude of such oscillations is sensitive to the laser frequency ω. In Ref. [25] a slightly greater laser frequency, $\omega = 1$ eV, resulted in $\sigma(\beta)$ oscillations having a magnitude of 2% from peak to trough [45]. Thus, by lowering the frequency to $\omega = 0.84$ eV, we are able to increase the magnitude of the oscillations by a factor of 5. The reason for this sensitivity may be deduced from the modulation factor $H(\xi)$ shown in Fig. 2. The scaled energy variable ξ is proportional to $(\omega + \epsilon_i)$. Hence, increasing ω from 0.84 eV to 1 eV changes ξ from about 3.9 to 11.2. One sees that $H(\xi)$ is oscillating with much greater amplitude near $\xi = 3.9$ than near $\xi = 11.2$ (which is just off the scale of Fig. 2).

A second observation is that $\sigma(\beta)$ oscillates at about one-half the magnitude that the long laser pulse limit for $H(\xi)$ does near the same frequency. For example, the peak to trough magnitude of the oscillation in $\sigma(\beta)$ of about 10% shown in Fig. 5 compares with a peak trough oscillation of about 20% in the 1 psec laser pulse curve for $H(\xi)$ near $\xi = 3.9$. [Similarly, the magnitude of oscillation in $\sigma(\beta)$ at $\omega = 1$ eV of about 2% found in Ref. [25] compares to an oscillation of about 4% in the 1 psec laser pulse curve for $H(\xi)$ near $\xi = 11.2$.] The reason for the factor of 2 difference stems from the use of a single, long laser pulse to calculate $H(\xi)$ vs two short laser pulses to calculate $\sigma(\beta)$. In the former case, nearly all of the electron probability amplitude is affected by interference between the direct path and the reflected path amplitudes. [Only probability amplitudes created within one reflection time of the front and back ends of the laser pulse do not experience such interference, and

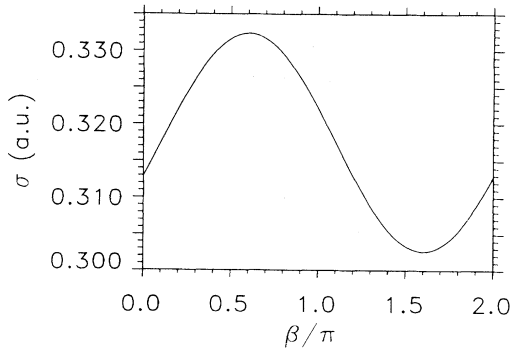

FIG. 5. Photodetachment cross section of the H^- ion in a uniform static electric field ($E_S = 1.64 \times 10^5$ V/cm directed along the z axis) by a double laser pulse of the form in Fig. 1(b) linearly polarized along the z axis. The cross section is shown for $\omega = 0.84$ eV as a function of the relative phase β of the two laser pulses. Each laser pulse has a width $2/\alpha = 0.06$ psec and they are separated by a time delay $\tau = 0.12$ psec.

these have very low amplitude because the laser pulse has low amplitude at its beginning and end.] On the other hand, the two short laser pulses (i.e., shorter than the reflection time in the electric field) each produce two wave packets, one that travels along the direct path and one that travels along the reflected path. The interference that can be varied by varying the relative phase β is that between the reflected path wave packet produced by the first short laser pulse and the direct path wave packet produced by the second short laser pulse. Hence only half the total wave-packet probability produced by the double laser pulse is affected by interference.

4. Dependence of the detachment cross section on the time delay between two short laser pulses: Ramsey fringes

In Fig. 6 we present the dependence of the photodetachment cross section on the time delay τ between the two short laser pulses [cf. Eq. (1)]. We plot curves of $\sigma(\tau)$ for two values of the relative phase between the laser pulses: $\beta = 0.6\pi$ and $\beta = 1.6\pi$. From Fig. 5 we see that at these two values of β, $\sigma(\beta)$ has respectively a maximum and a minimum. Thus Fig. 6 represents an envelope within which all possible behaviors for different values of β are encompassed.

Various features of Fig. 6 may be understood by close examination of Eq. (1). First, for $\tau = 0$ the cross section becomes independent of the relative phase β. This independence is because the part of the double laser pulse in Eq. (1) which results in photon absorption differs from that for the single laser pulse in Eq. (2) by the factor $1+e^{-i\beta}$. The absolute square of this factor is $2(1+\cos\beta)$, which is precisely the difference between the photon flux F_2 for the double laser pulse in Eq. (36) and F_1 for the single laser pulse in Eq. (34).

Second, the time delay $\tau = 4/\alpha$ marks the dividing point between laser pulses which overlap and those which do not. This may be seen from Fig. 1(b), which plots Eq.

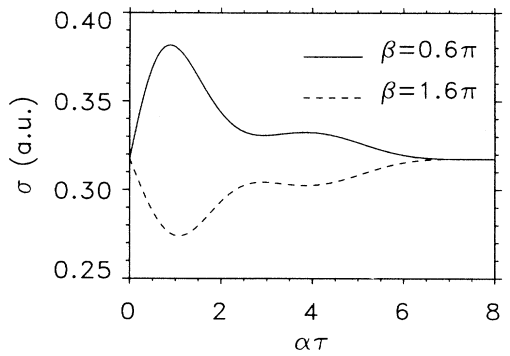

FIG. 6. Photodetachment cross section of the H^- ion in a uniform static electric field ($E_S = 1.64 \times 10^5$ V/cm directed along the z axis) by a double laser pulse of the form in Fig. 1(b) linearly polarized along the z axis. The cross section is shown for $\omega = 0.84$ eV as a function of the time delay τ of the two laser pulses for two values of the relative phase β [cf. Eq. (1)]. Each laser pulse has a width $2/\alpha = 0.06$ psec.

(1) for the case $\tau = 4/\alpha$. For $\tau < 4/\alpha$ the two pulses overlap, while for $\tau \geq 4/\alpha$ they do not. Since we have chosen the laser frequency $\omega = 0.84$ eV in calculating Fig. 6, the classical reflection time equals $4/\alpha = 0.12$ psec. Hence $\sigma(\tau)$ for $4/\alpha \leq \tau \leq 8/\alpha$ decreases from a local maximum for $\beta = 0.6\pi$ (minimum for $\beta = 1.6\pi$) to a constant value independent of β for values of τ much greater than the classical reflection time T_E; i.e., for $\tau \gg T_E$, no interference occurs and hence the cross section is not sensitive to β. In fact, it approaches the single laser pulse cross section. (Note that since our calculation ignores the final-state interaction of the detached electron with the H atom, there are no revivals of cross-section oscillations for values of τ equal to multiples of T_E; this approximation is a common and good one for weak laser-field detachment of H^- in a static electric field [46].)

Note that Ramsey fringes [47] would normally be expected in a plot such as that shown in Fig. 6 (e.g., cf. Refs. [17,26]). The absence of such fringes therefore requires explanation. Ramsey's key idea [47] is exactly the one we are employing, namely, to have a quantum-mechanical system pass *twice* through a region, having an electromagnetic field and to study the consequences of varying the relative phases between the two passages. The details of the case in Ref. [47] and the present case are different, however, and worth describing briefly.

The classic Ramsey experiment is to send a beam of molecules along a path through a region in which they experience *the same* electromagnetic field at each end of the region, but not in the middle [47]. Ramsey showed that one gets a resonance in the signal power absorbed by the molecules in the second field region as a function of the detuning $\omega - \omega_0$, where ω is the electromagnetic field frequency and ω_0 is the frequency of the molecular transition from the ground state. This resonance comes about because during the time T that the molecules pass from one region of the electromagnetic field to the other, their dipole moment acquires a phase $\omega_0 T$. During this same time, however, the field acquires a phase ωT. The phase difference is thus $(\omega - \omega_0)T$. By varying ω one can therefore accurately determine ω_0.

In this paper we are considering detachment of a negative ion in one or more static external fields. Since we are in the continuum, we always have $\omega_0 = \omega$. In our double laser pulse calculations, the time delay τ [cf. Eq. (1)] corresponds to the transit time T in a classical Ramsey experiment. The relative phase β in Eq. (1) between the two laser pulses corresponds to the phase difference $(\omega - \omega_0)T$ in a classical Ramsey experiment. For simplicity in our calculations, we have chosen β to be a parameter independent of ω and τ. The result for $\sigma(\tau)$ shown in Fig. 6 depends on this simplifying assumption.

In a real experiment, we do expect there to be Ramsey fringe-type behavior in a measurement of $\sigma(\tau)$ vs τ. In our work we have employed the electric dipole approximation for the usual reason, namely, that the laser wavelength is much larger than the interaction region relevant to photodetachment. That is, we have neglected the phase factor $\vec{k}\cdot\vec{r}$ in describing our laser pulses. However, in order to create the coherent double laser pulse described by Eq. (1) in practice, we imagine that one

would need to split a single laser pulse and delay one of the split beams by reflecting it around the laboratory. Of course, over distances of macroscopic size, the phase $\vec{k}\cdot\vec{r}$ cannot be neglected. Since $k=\omega/c$ and $r=c\tau$, it is clear that delaying a laser pulse by reflecting it around the laboratory will introduce a phase difference that includes a term of the form $\omega\tau$. Indeed, our double laser pulse described by Eq. (1) essentially agrees with that in Eq. (1) of Ref. [17] if we set $\beta=-\omega\tau$.

Thus, whereas the plots of $\sigma(\tau)$ vs τ presented in Fig. 6 are correct for the two constant values of β chosen, in practice it is likely that the price of delaying one of the laser pulses by τ is to introduce a relative phase that includes a term of the form $\omega\tau$. Such a relative phase would result in a rapid oscillation confined within the envelope in Fig. 6 represented by the two curves for the extreme values of β. Similar remarks apply to Fig. 15. No other figures in this paper are affected by such Ramsey fringes. Because all other calculations in this paper employing the double laser pulse in Eq. (1) are carried out for fixed ω and τ, a relative phase of the form $\omega\tau$ simply contributes a constant phase within the overall relative phase β. The phase difference β may, of course, be varied even with fixed ω and τ by passing the second laser pulse through a phase-changing medium.

B. Parallel static electric- and magnetic-field case

In the preceding subsection we have presented calculations that demonstrate that one can increase the magnitude of quantum interference effects in photodetachment of H^- in a static, uniform electric field by using laser detachment frequencies closer to the detachment threshold [cf. Fig. 2]. However, the threshold is generally where the cross-section magnitude is smallest. In our calculations at $\omega=0.84$ eV (i.e., only 85 meV above threshold) the amount of interference controllable with two coherent, short laser pulses is only enough to create about a 10% variation in the cross section [cf. Fig. 5]. This modest variation stems from the fact that the detached electron probability amplitude created by short laser pulses is free to spread in the direction perpendicular to the static, uniform electric field. In this section we show that use of a parallel magnetic field to reflect the detached electron probability amplitude back to the origin permits far greater control of the detachment cross section magnitude with coherent short laser pulses.

1. Detachment cross section and modulation factor dependence on laser pulse duration

In our calculations we choose $B=1$ T, which results in a classical period for motion perpendicular to the field of

$$T_B=2\pi/\omega_c=35.72\ \text{psec}. \tag{55}$$

The static electric-field magnitude is chosen so that the classical reflection time [cf. Eq. (54)] along the z axis is of comparable magnitude to T_B near the detachment threshold. We have chosen $E_S=60$ V/cm^{-1}. In Fig. 7 we present the detachment cross sections produced by a single laser pulse [cf. Eq. (2) and Fig. 1(a)] for various static field configurations (E_S only, B only, and $E_S \parallel B$) and two laser pulse widths $2/\alpha$. In Fig. 8 we present the modulation factors [cf. Sec. II H] corresponding to the cross sections in Fig. 7.

One sees clearly in Figs. 7(a) and 8(a) that the cross section produced by a relatively long laser pulse (i.e., $2/\alpha=500$ psec as compared to the classical reflection time T_B of 35.7 psec) shows much greater interference than detachment in either a pure E_S field or a pure B field. Furthermore, Fig. 8(a) clearly shows evidence of a "revival" of the amplitude of the modulation factor at a frequency above threshold of about 11 cm^{-1}, for which $T_E\approx T_B$. (We shall discuss such revivals in more detail below.) Note, however, that when the laser pulse width is chosen to be shorter than both the electric-field period T_E and the magnetic-field period T_B (i.e., $2/\alpha=T_B/2=17.86$ psec), then the quantum interference disappears, as shown in Figs. 7(b) and 8(b).

Our long laser pulse results for the cross section and modulation factor in the parallel fields case agree well with the monochromatic field results presented in Refs. [31] and [32]. In particular, we have chosen E_S and B values equal to those selected in Fig. 1(c) of Ref. [31]. A comparison of this latter figure with our result in Fig. 8(a) for the modulation factor shows good quantitative agreement. However, our results are smoother, without

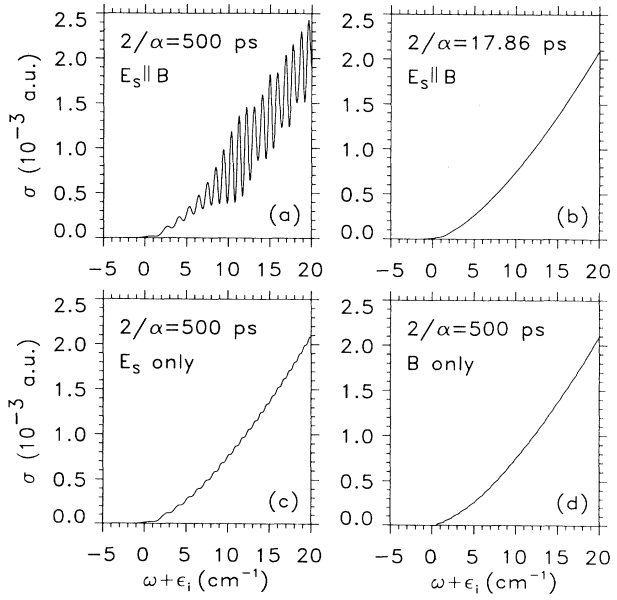

FIG. 7. (a) Photodetachment cross section of the H^- ion in parallel static electric ($E_S=60$ V/cm) and magnetic ($B=1$ T) fields plotted vs energy (in cm^{-1} above the zero-field threshold) for a single laser pulse [cf. Eq. (2) and Fig. 1(a)] having width $2/\alpha=500$ psec. (b) Same as (a) for laser pulse width $2/\alpha=17.86$ psec. (c) Same as (a), but with $B=0$. (d) Same as (a), but with $E_S=0$.

the kinks and spikes shown in Ref. [31]. We suspect that these kinks and spikes are spurious numerical effects.

2. *Time dependence of detached electron wave packets*

Our results for the detached electron probability density produced by a single short laser pulse of the form of Eq. (2) [cf. Fig. 1(a)] are shown in Figs. 9 and 10. We plot in these figures contours of a normalized wave-packet probability density $|\psi_{\rm WP}(x,p_y,z,t)|^2/(2\pi F_1)$ as a function of x and z for $p_y = 0$ and for various times t, which are measured in units of $1/\alpha$ [cf. Eq. (2) and Fig. 1(a)]. The wave packet $\psi_{\rm WP}$ is defined by Eq. (24) and the flux F_1 by Eq. (34). Division of $|\psi_{\rm WP}|^2$ by F_1 gives results that are independent of the laser amplitude E_0 in the weak laser limit [cf. Eqs. (24), (23a), (39), and (34)]. [Note also that the cross section is equal to $|\psi_{\rm WP}|^2/(2\pi F_1)$ integrated over x, p_y, and z in the limit that $t \to \infty$.] One sees in Fig. 9 that at $\alpha t = -1.0$, the probability is just beginning to be noticeable. For $-0.5 \le \alpha t \le 1.0$, the probability amplitude grows in magnitude and proceeds to bifurcate. By $\alpha t = 1.5$ there are two well-separated wave packets, one proceeding along the direct path toward negative z and the other being reflected by the Stark potential barrier at positive z.

Figure 10 shows the time development of the wave packets produced by a single, short laser pulse after the pulse has passed over the H^- ion (i.e., for $\alpha t \ge 2.0$). Figures 10(a) and 10(b) show how the direct path probability density escapes along the negative z axis, narrowing its width along the x axis as it does so. Figures 10(c)–10(f) illustrate how the reflected path probability density returns to the origin and then proceeds to escape along the negative z axis. It is delayed by a time $4/\alpha$ compared to the direct path probability density.

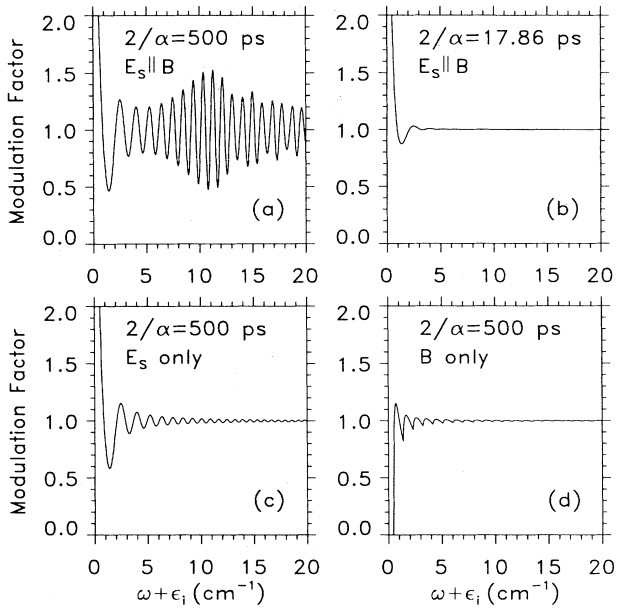

FIG. 8. Modulation factors $H(E_S,B)$ [cf. Eqs. (48) and (49)] corresponding to the cross sections in Figs. 7(a)–7(d).

Figures 11 and 12 demonstrate how one can partially control the magnitude of the detached electron probability density which escapes along the negative z axis by employing a coherent, double laser pulse of the kind defined by Eq. (1) and exhibited in Fig. 1(b). In these figures we plot the normalized wave packet probability

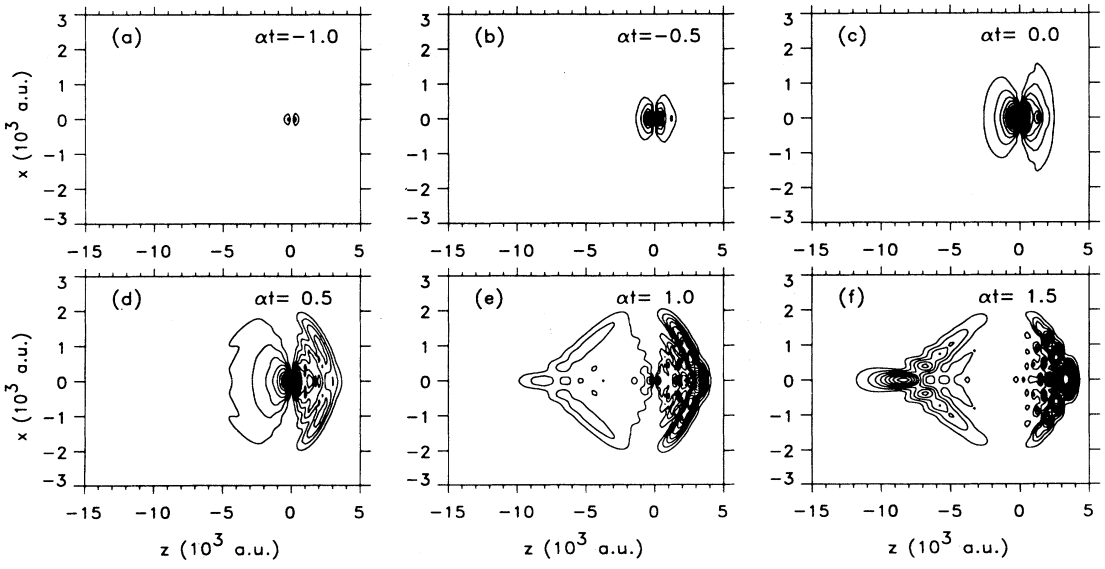

FIG. 9. Contour plots of the normalized wave-packet probability density $|\psi_{\rm WP}(x,p_y=0,z,t)|^2/(2\pi F_1)$ as a function of x and z produced by a short single laser pulse [cf. Eq. (2) and Fig. 1(a)] of width $2/\alpha = 17.86$ psec and flux F_1 [cf. Eq. (34)]. The wave packet is shown at the following times t: (a) $-1.0/\alpha$, (b) $-0.5/\alpha$, (c) 0.0, (d) $0.5/\alpha$, (e) $1.0/\alpha$, and (f) $1.5/\alpha$. At these times the laser pulse is passing over the H^- ion. The laser frequency is 10 $\rm cm^{-1}$ above the zero-field ionization threshold.

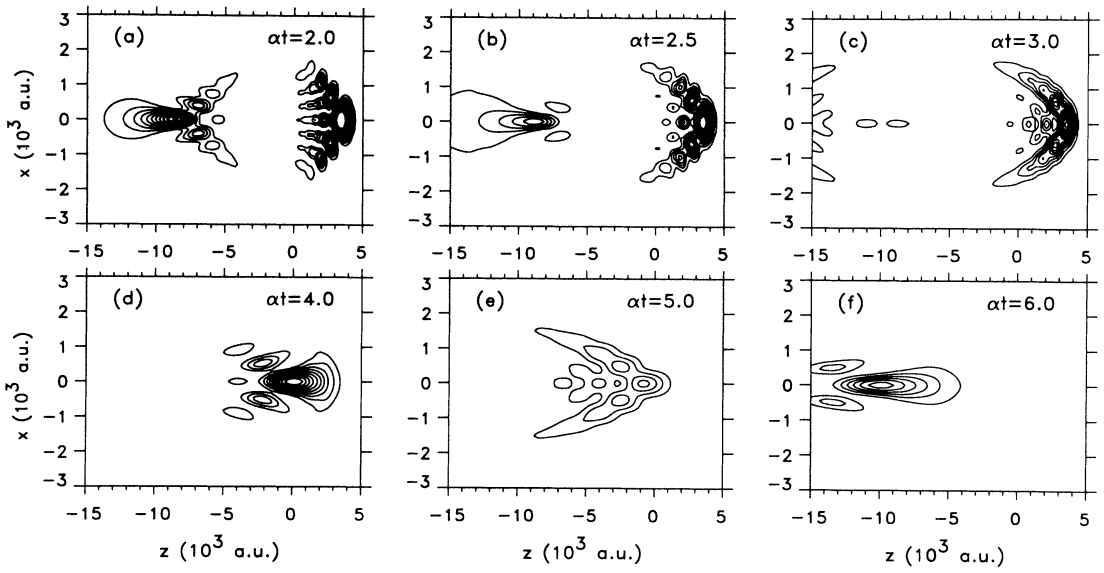

FIG. 10. Same as in Fig. 9 for times t after the laser pulse has passed over the H^- ion. The wave packet is shown at the following times t: (a) $2.0/\alpha$, (b)$2.5/\alpha$, (c) $3.0/\alpha$, (d) $4.0/\alpha$, (e) $5.0/\alpha$, and (f) $6.0/\alpha$.

density $|\psi_{\rm WP}(x,p_y,z,t)|^2/(2\pi F_2)$. The two laser pulses have a separation $\tau = 4/\alpha$ equal to the wave-packet reflection time $T_B \approx T_E$; their relative phase β is 0.7386π in Fig. 11 and 1.7386π in Fig. 12. Figure 11 shows the case of constructive interference between the probability amplitudes, while Fig. 12 shows the case of destructive interference for times $3.5/\alpha \leq t \leq 6.0/\alpha$, during which the second laser pulse is on [cf. Fig. 1(b)]. Note that the reflected path probability density produced by the second laser pulse [cf. Figs. 11(f) and 12(f)] will proceed along the negative z axis much as that produced by the single laser pulse does in Fig. 10, but with a time delay of $\Delta t = 4.0/\alpha$.

Figure 13 shows three-dimensional plots of the normal-

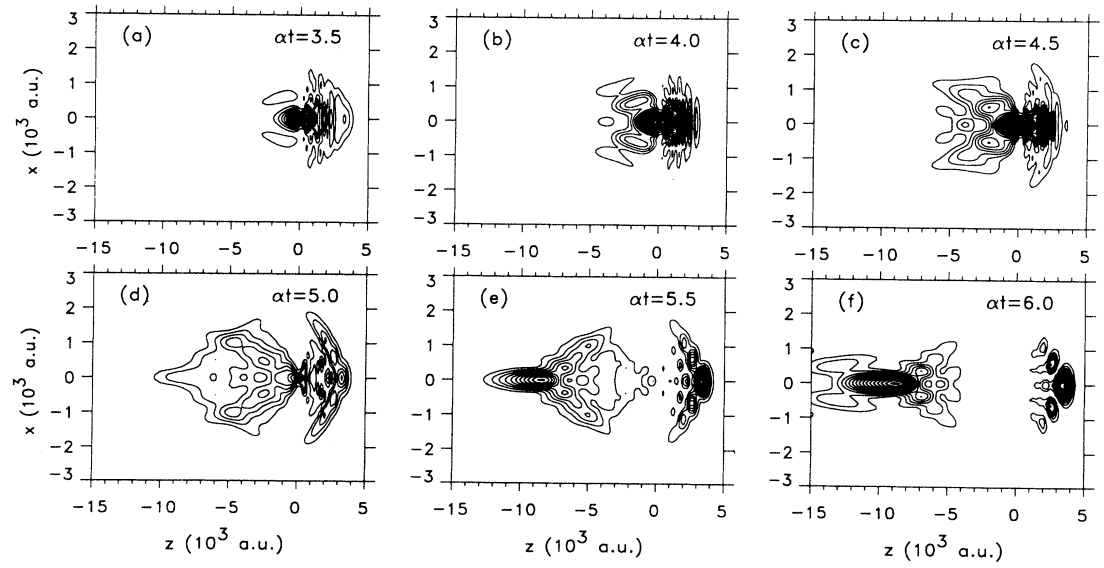

FIG. 11. Contour plots of the normalized wave-packet probability density $|\psi_{\rm WP}(x,p_y=0,z,t)|^2/(2\pi F_2)$ as a function of x and z produced by two coherent laser pulses [cf. Eq. (1) and Fig. 1(b)] of width $2/\alpha = 17.86$ psec, pulse separation $\tau = 4/\alpha = 35.72$ psec, flux F_2 [cf. Eq. (36)], and relative phase $\beta = 0.7386\pi$ (which leads to constructive interference). The wave packet is shown at the following times t: (a) $3.5/\alpha$, (b) $4.0/\alpha$, (c) $4.5/\alpha$, (d) $5.0/\alpha$, (e) $5.5/\alpha$, and (f) $6.0/\alpha$. At these times the reflected path wave packet produced by the first laser pulse is returning to the origin just as the second laser pulse is passing over the H^- ion. The laser frequency is 10 $\rm cm^{-1}$ above the zero-field ionization threshold.

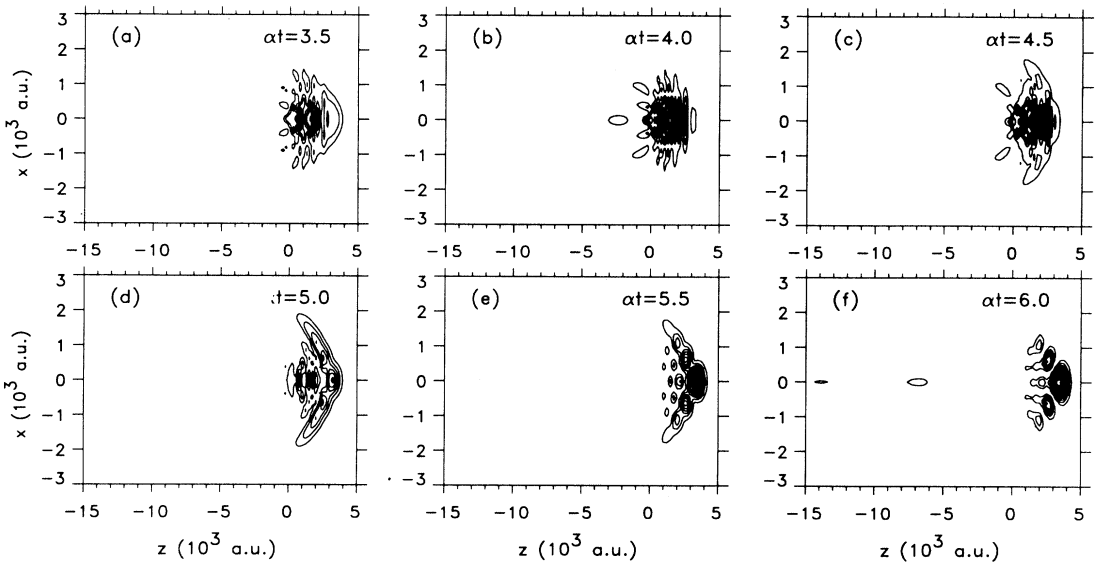

FIG. 12. Same as Fig. 11, except that the relative phase $\beta = 1.7386\pi$ (which leads to destructive interference).

ized detached electron probability densities at $t = 6.0/\alpha$ for the three cases shown in two dimensions in Figs. 10(f), 11(f), and 12(f). Thus Fig. 13(a) shows the reflected path probability density produced by a single laser pulse proceeding along the negative z axis. Figures 13(b) and 13(c) show how this reflected path probability density produced by a first laser pulse is affected when its amplitude undergoes constructive and destructive interference, respectively, with the electron probability amplitude produced by a second short laser pulse.

3. Dependence of the detachment cross section on the relative phase and time delay between two short laser pulses

The wave-packet calculations shown in the preceding subsection employed the value $p_y = 0$ in $\psi_{\rm WP}(x, p_y, z, t)$. The cross section [cf. Eq. (28)] sums over all final states and hence is expected to show smaller quantum interference effects than do the individual wave packets (for which the values of β were chosen to produce the maximum amount of interference). Nevertheless, Fig. 14 shows that $\sigma(\beta)$ has a peak to trough variation of about 50% of its average value.

It is interesting to compare the magnitude of this variation with that for the pure static electric-field case. For $E_S = 60$ V/cm and $\omega + \epsilon_i = 10$ cm^{-1}, the scaled energy variable ξ [cf. Eq. (38)] takes the value 11.2, which is exactly the same as considered in Ref. [25] in a pure static electric-field case (for $E_S = 1.64 \times 10^5$ V/cm and $\omega = 1$ eV). However, in that case the variation of $\sigma(\beta)$ about its mean value was of the order of only 2%. The introduction of a magnetic field has increased the vari-

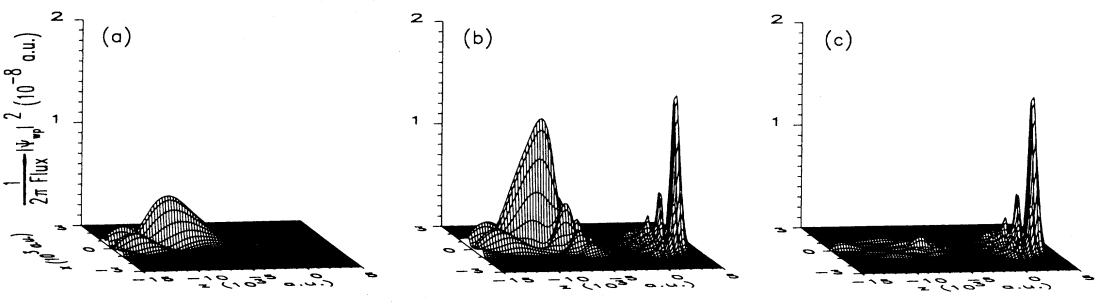

FIG. 13. Comparison of the normalized wave-packet probability densities $|\psi_{\rm WP}(x, p_y = 0, z, t)|^2/(2\pi F)$ as a function of x and z produced by three different types of short laser pulses having a frequency that is 10 cm^{-1} above the zero-field ionization threshold and characterized by the width $2/\alpha = 17.86$ psec and flux F [cf. Eqs. (34 and 36)]. All figures are for a time $t = 6.0/\alpha$ after the laser pulse has passed over the H$^-$ ion. (a) Single short laser pulse case shown in contour in Fig. 10(f). (b) Double laser pulse case (illustrating constructive interference) shown in contour in Fig. 11(f). (c) Double laser pulse case (illustrating destructive interference) shown in contour in Fig. 12(f).

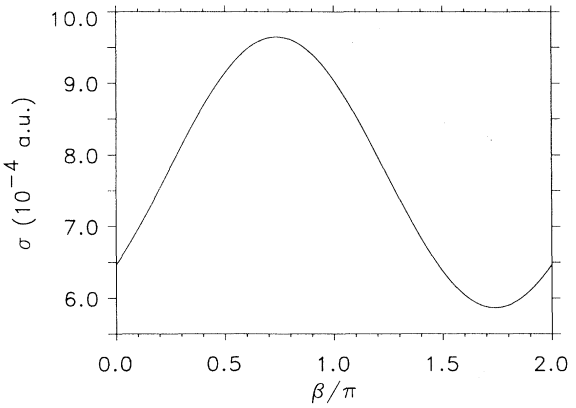

FIG. 14. Photodetachment cross section of the H^- ion in parallel static electric ($E_S = 60$ V/cm) and magnetic ($B = 1$ T) fields by a double laser pulse of the form in Fig. 1(b) linearly polarized along the static field axis. The cross section is shown for a frequency 10 cm^{-1} above the zero-field ionization threshold as a function of the relative phase β of the two laser pulses. Each laser pulse has a width $2/\alpha = 17.86$ psec and they are separated by $\tau = 35.72$ psec.

ation to 50%. As shown in Fig. 5, even a more optimal static electric-field case (having $\xi = 3.9$) only produces variations of $\sigma(\beta)$ of the order of 10%. Clearly, the parallel magnetic field makes it possible to exert much greater control over $\sigma(\beta)$ through variation of the relative phase β. (Note that theoretical calculations for detachment in a pure static magnetic-field case show interference effects of about 20% of the total detachment cross section [26].)

In Fig. 15 we show the dependence of the photodetachment cross section on the time delay τ between two short laser pulses [cf. Eq. (1)]. Plotted are curves of $\sigma(\tau)$ for two values of the relative phase between the laser pulses:

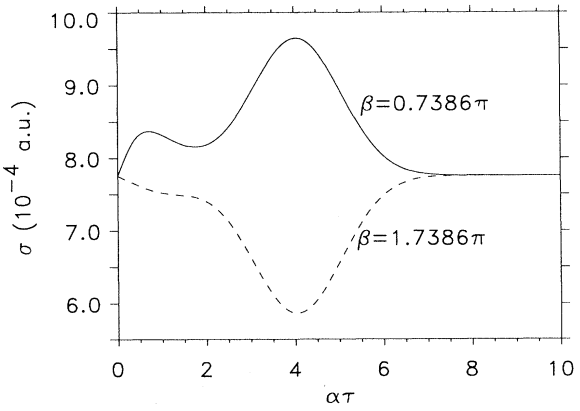

FIG. 15. Photodetachment cross section of the H^- ion in parallel static electric ($E_S = 60$ V/cm) and magnetic ($B = 1$ T) fields by a double laser pulse of the form in Fig. 1(b) linearly polarized along the static field axis. The cross section is shown for a frequency 10 cm^{-1} above the zero-field ionization threshold as a function of the time delay τ of the two laser pulses for two values of the relative phase β [cf. Eq. (1)]. Each laser pulse has a width $2/\alpha = 0.06$ psec.

$\beta = 0.7386\pi$ and $\beta = 1.7386\pi$. As shown in Fig. 14, at these two values of β the cross section $\sigma(\beta)$ has, respectively, a maximum and a minimum. Thus Fig. 15 represents an envelope within which all possible behaviors for different values of β are encompassed.

Details of Fig. 15 are similar to those in Fig. 6. These details are discussed in Sec. III A 4. In particular, in an actual experimental measurement, Ramsey fringes with frequency ω are expected to fill the envelope in Fig. 15. The "width" of the envelope in Fig. 15 at a time delay $\tau = 4/\alpha$ is approximately 50% of the average value of the cross section for large values of τ. This is five times greater than the width shown in Fig. 6 for a pure static electric-field case.

4. Cross-section revivals

As mentioned in the Introduction, one of the most interesting features of the parallel static electric and magnetic-field problem is that there are two time scales for wave-packet motion: the period T_E for motion along the positive z axis and the period T_B for motion perpendicular to the z axis. These two periods are the times needed for the detached electron wave packet to be reflected back to the origin by the static electric and magnetic fields, respectively. Classically T_E is given by Eq. (54) with $\epsilon_\perp \equiv \omega_c(n+1/2)$. Hence $T_E(n,\omega)$ is a function of the Landau level n ($\omega_c = 0.934$ cm^{-1} or 116 meV for $B = 1$ T) as well as the laser frequency ω. T_B is given by

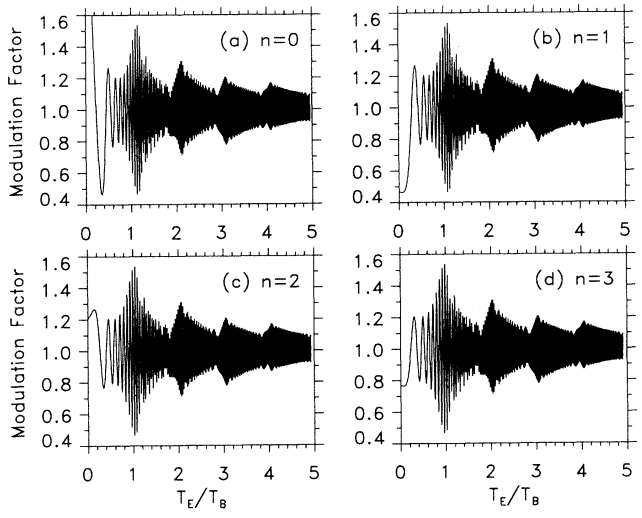

FIG. 16. Modulation factors [cf. Eq. (48)] corresponding to the total photodetachment cross sections σ [cf. Eq. (29)] for H^- in parallel static electric ($E_S = 60$ V/cm) and magnetic ($B = 1$ T) fields by a linearly polarized laser pulse [cf. Eq. (2) and Fig. 1(a)] of width $2/\alpha = 500$ psec. Modulation factors are plotted vs the ratio of reflection times for motion along and perpendicular to the z axis, $T_E(n,\omega)/T_B$, for particular Landau channels n. Note that $T_B = 35.7$ psec and $T_E(n,\omega)$ is a function of laser frequency ω. (a) $n = 0$, (b) $n = 1$, (c) $n = 2$, and (d) $n = 3$.

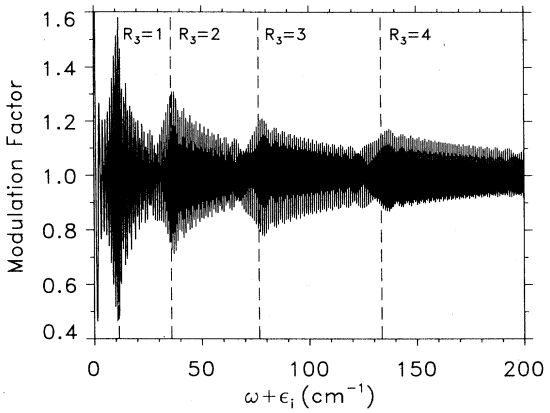

FIG. 17. Modulation factor [cf. Eq. (48)] for the total detachment cross section σ [cf. Eq. (29)] plotted versus the energy $(\omega + \epsilon_i)$ above the zero-field ionization threshold. The static and laser fields are the same as in Fig. 16. The dashed lines indicate the locations of integer values of the ratio $R_3 \equiv T_E(n = 3, \omega)/T_B$, where T_E and T_B are the reflection times for motion along and perpendicular to the z axis. The ratio R_n for the $n = 3$ Landau level gives the best match with peak amplitudes in the modulation factor, as shown in Fig. 16.

Eq. (55) and is independent of the Landau level and the laser frequency.

One expects naively to be able to control the magnitude of the detachment cross section best when the reflected wave-packet amplitudes traveling along the positive z axis and perpendicular to the z axis coincide back at the origin. Evidence for such revivals in the cross section is presented in Fig. 16. In this figure we plot the modulation factors [cf. Eq. (48)] corresponding to the total cross sections σ [cf. Eq. (29)] as a function of the ratio $T_E(n, \omega)/T_B$ for the Landau levels n=0,1,2,3. It is clear that the modulation factors exhibit revivals of their amplitude whenever $T_E(n, \omega)$ is close to an integer multiple of T_B. As shown, the ratio for $n = 3$ gives the best match with the peaks in the modulation factor for the total cross section. (Note that the partial cross sections σ_n [cf. Eq. (29)] do not exhibit revivals. According to Eq. (46) these partial cross sections simply show primarily the oscillations of the derivative of the Airy function.) Hence the classical notion of a period for motion in a particular direction is found to be useful for interpreting our quantum-mechanical results for the total cross section even for the long-pulse limit in which the laser pulse width in energy is smaller than ω_c.

In Fig. 17 we present the modulation factor for the total cross section [cf. Eq. (29)] as a function of laser frequency above the zero-field ionization threshold. The dashed lines show the frequency locations of integer values of the ratio $R_3 \equiv T_E(n = 3, \omega)/T_B$, as this ratio was shown in Fig. 16 to match best with the revivals in the total cross section. Of course, all Landau levels n contribute to σ. Note that our results in Figs. 9–14 are computed for $(\omega + \epsilon_i) = 10$ cm^{-1}, which corresponds to $R_1 = 1$.

IV. SUMMARY AND CONCLUSIONS

In this paper we have shown how one may control continuum electron wave packets using static fields and coherent short-pulse lasers. Using the H⁻ ion as a prototype system and analytic, three-dimensional final-state wave functions for electrons moving in both static and laser fields we have presented photodetachment cross sections, modulation factors, and detached electron wave-packet results in both static electric and parallel electric and magnetic fields. Throughout our presentation, we have shown how the modulation factors characterizing near-threshold cross sections resulting from detachment by relatively long laser pulses may be employed to set the parameters for short laser pulses in order to optimize the extent of quantum interference effects (where short and long are in comparison with classical reflection times).

A key conclusion of this work is that control of the spreading of continuum electron wave packets is essential to producing quantum interference effects of significant amplitude in the total detachment cross sections. Use of a static magnetic field to control spreading perpendicular to the z axis is shown to be ideal for this purpose. Even when one optimizes short-pulse laser parameters in the case of a pure static electric field, the quantum interference effects are of modest magnitude (of the order of 10% for the parameters chosen in this paper). By contrast, use of parallel static magnetic and electric fields allows achievement of quantum interference effects of the order of 50% of the detachment cross section.

Finally, as was emphasized in Ref. [25], our calculations indicate a new type of experiment: control of the magnitude of photodetachment at any convenient laser frequency through use of coherent short laser pulses having variable relative phase.

ACKNOWLEDGMENT

This work was supported in part by NSF Grant No. PHY-9410850.

[1] D. J. Tannor and S. A. Rice, J. Chem. Phys. **83**, 5013 (1985).
[2] D. J. Tannor, R. Kosloff, and S. A. Rice, J. Chem. Phys **85**, 5805 (1986).
[3] D. J. Tannor and S. A. Rice, Adv. Chem. Phys. **70**, 441 (1988).
[4] P. Brumer and M. Shapiro, Chem. Phys. Lett. **126**, 541 (1986).
[5] M. Shapiro, J. W. Hepburn, and P. Brumer, Chem. Phys. Lett. **149**, 451 (1988).
[6] P. Brumer and M. Shapiro, Acc. Chem. Res. **22**, 407 (1989).

[7] S. P. Lu, S. M. Park, Y. Xie, and R. J. Gordon, J. Chem. Phys. **96**, 6613 (1992).
[8] G. Alber and P. Zoller, Phys. Rep. **199**, 231 (1991).
[9] See, e.g., E. J. Heller and S. Tomsovic, Phys. Today **46** (7), 38 (1993), and references therein.
[10] J. Parker and C. R. Stroud, Jr., Phys. Rev. Lett. **56**, 716 (1986).
[11] J. A. Yeazell and C. R. Stroud, Jr., Phys. Rev. A **35**, 2806 (1987); Phys. Rev. Lett. **60**, 1494 (1988).
[12] H. G. Muller, P. H. Bucksbaum, D. W. Schumacher, and A. Zavriyev, J. Phys. B **23**, 2761 (1990).
[13] A. Szöke, K. C. Kulander, and J. N. Bardsley, J. Phys. B **24**, 3165 (1991).
[14] R. M. Potvliege and P. H. G. Smith, J. Phys. B **24**, L641 (1991).
[15] T. Nakajima and P. Lambropoulos, Phys. Rev. Lett. **70**, 1081 (1993).
[16] G. Alber, H. Ritsch, and P. Zoller, Phys. Rev. A **34**, 1058 (1986).
[17] L. D. Noordam, D. I. Duncan, and T. F. Gallagher, Phys. Rev. A **45**, 4734 (1992).
[18] G. Alber, Phys. Rev. A **40**, 1321 (1989).
[19] G. Alber, Z. Phys. D **14**, 307 (1989).
[20] G. Alber, Comments At. Mol. Phys. **26**, 47 (1991).
[21] A. ten Wolde, L. D. Noordam, A. Lagendijk, and H. B. van Linden van den Heuvell, Phys. Rev. A **40**, R485 (1989).
[22] B. Broers, J. F. Christian, J. H. Hoogenraad, W. J. van der Zande, H. B. van Linden van den Heuvell, and L. D. Noordam, Phys. Rev. Lett. **71**, 344 (1993).
[23] J. C. Gay, D. Delande, and A. Bommier, Phys. Rev. A **39**, 6587 (1989).
[24] J. A. Yeazell, G. Raithel, L. Marmet, H. Held, and H. Walther, Phys. Rev. Lett. **70**, 2884 (1993).
[25] Q. Wang and A. F. Starace, Phys. Rev. A **48**, R1741 (1993).
[26] I. Y. Kiryan and D. J. Larson, Phys. Rev. Lett. **73**, 943 (1994).
[27] I. I. Fabrikant, Zh. Eksp. Teor. Fiz. **79**, 2070 (1980) [Sov. Phys. JETP **52**, 1045 (1980)].
[28] W. P. Reinhardt, in *Few-Body Systems and Multiparticle Dynamics,* Proceedings of the Symposia of the Topical Group on Few-Body Systems and Multiparticle Dynamics, AIP Conf. Proc. No. 162, edited by D. A. Micha (AIP, New York, 1987), pp. 94–110.
[29] H. C. Bryant, in *Atomic Spectra and Collisions in External Fields,* edited by K. T. Taylor, M. H. Nayfeh, and C. W. Clark (Plenum, New York, 1988).
[30] H. C. Bryant, A. Mohagheghi, J. E. Stewart, J. B. Donahue, C. R. Quick, R. A. Reeder, V. Yuan, C. R. Hummer, W. W. Smith, S. Cohen, W. P. Reinhardt, and L. Overman, Phys. Rev. Lett. **58**, 2412 (1987).
[31] M. L. Du, Phys. Rev. A **40**, 1330 (1989).
[32] I. I. Fabrikant, Phys. Rev. A **43**, 258 (1991).
[33] A. Peters and J. B. Delos, Bull. Am. Phys. Soc. **39**, 1075 (1994).
[34] B. Gao, Phys. Rev. A **41**, 5039 (1990).
[35] B. Gao and A. F. Starace, Phys. Rev. A **42**, 5580 (1990).
[36] D. M. Volkov, Z. Phys. **94**, 250 (1935).
[37] L. D. Landau and E. M. Lifshitz, *Quantum Mechanics,* 2nd ed. (Pergamon, Oxford, 1965), pp. 70 and 71.
[38] T. Ohmura and H. Ohmura, Phys. Rev. **118**, 154 (1960).
[39] H. A. Bethe and C. Longmire, Phys. Rev. **77**, 647 (1950).
[40] The determination of the value of b for H^- is discussed briefly on p. 5588 of Ref. [35] and in detail by M. L. Du and J. B. Delos, Phys. Rev. A **38**, 5609 (1988).
[41] I. S. Gradshteyn and I. M. Ryzhik, *Tables of Integrals, Series and Products* (Academic, New York, 1965), Sec. 7.374(1).
[42] Bo Gao, Ph.D. thesis, The University of Nebraska–Lincoln, 1989. See Appendix D, Sec. D.1(a), Eq. (D.25).
[43] E. P. Wigner, Phys. Rev. **73**, 1002 (1948).
[44] *Handbook of Mathematical Functions,* edited by M. Abramowitz and I. A. Stegun (Dover, New York, 1965), Eqs. 10.4.60 and 10.4.62.
[45] Compare Fig. 5 of Ref. [25].
[46] See Ref. [35] and references therein.
[47] N. F. Ramsey, Phys. Rev. **78**, 695 (1950). See also the nice discussion in W. Demtröder, *Laser Spectroscopy* (Springer, Berlin, 1988), pp. 612–615.